Supplementary to

Experimental thermodynamic study of the "high-entropy" oxide $(MgCoNiCuZn)_{0.2}O$: entropic stabilization confirmed, but is it all that matters?

Vladimir V. Sereda [a,*], Dmitry S. Tsvetkov [a], Anna V. Sereda [a],
Dmitry A. Malyshkin [a], Irina A. Bajenova [b,c], Ivan L. Ivanov [a], Andrey Yu. Zuev [a]

[a] Institute of Natural Sciences and Mathematics,
Ural Federal University, 620002, 19 Mira St., Ekaterinburg, Russia

[b] Department of Chemistry,
Lomonosov Moscow State University, 1-3 Leninskiye Gory, 119991, Moscow, Russia

[c] Department "Master's School of Information Business Systems",
NUST MISIS, Leninsky Prospect 4, Moscow, 119049, Russian Federation

* corresponding author, vladimir.sereda@urfu.ru

1 Abbreviations

XRD – X-ray diffraction
EDS – energy-dispersive microanalysis
SEM – scanning electron microstopy
SE – secondary electrons
BSE – backscattered electrons
DSC – differential scanning calorimetry

Note: unless explicitly stated otherwise, the values of uncertainties and the values following the symbol "±" correspond to the combined expanded standard uncertainties with the coverage factor $k = 2$, which corresponds to the confidence level of ≈95%

1 Synthesis, chemical and phase analysis, and crystal structure (SEM-EDS and XRD)

Table S1. Chemical compounds used in the present work [a]

Chemical name	Source	Mass fraction purity	Analysis method
Al_2O_3 (powder, for DSC calibration)	Duksan Pure Chemicals	>0.997	Stated by the supplier
Al_2O_3 (monocrystalline sapphire, NIST SRM 720, for calibrating the drop calorimeters)	NIST	>0.9995	
Ga	Khimkraft	>0.9999	
In	Setaram	>0.99995	
Sn		>0.99999	
Pb		>0.99999	
Al		>0.99999	
Ag		>0.9999	
MgO	Reakhim	>0.999	
Co_3O_4	MCP HEK GmbH	>0.9997	
NiO	Ural'skiy zavod khimreaktivov	>0.9999	
CuO	Reakhim	>0.9999	
ZnO	Khimreaktivsnab	>0.995	
$(MgCoNiCuZn)_{0.2}O$	synthesis	>0.99	XRD, SEM, EDS

[a] purification methods were not used for any of the substances

Table S2. Rietveld-refined unit cell parameters and atomic coordinates for $(MgCoNiCuZn)_{0.2}O$ at 298 K and 100 kPa [a]

Unit cell parameters and unit cell volume					
Oxide	Space group	a / Å	b / Å	c / Å	V / Å^3
$(MgCoNiCuZn)_{0.2}O$	$Fm\bar{3}m$	4.2309	4.2309	4.2309	75.735
Atomic coordinates					
Oxide	Atom	x	y	z	Occupancy
$(MgCoNiCuZn)_{0.2}O$	M	0.5	0.5	0.5	0.00417
	O	0.0	0.0	0.0	0.02083

[a] Expanded standard uncertainties (≈95% confidence level) U are $U(a) = U(b) = U(c) = 0.0006$ Å, $U(V) = 0.04$ Å^3, $U(T) = 5$ K, $U(p) = 3$ kPa. Since we assume random mixing, the coordinates and occupancies of all cations in $(MgCoNiCuZn)_{0.2}O$ are the same. Thus, these parameters are listed in the "M" row in the table to avoid repetition. The temperature factors and the occupancies were not varied.

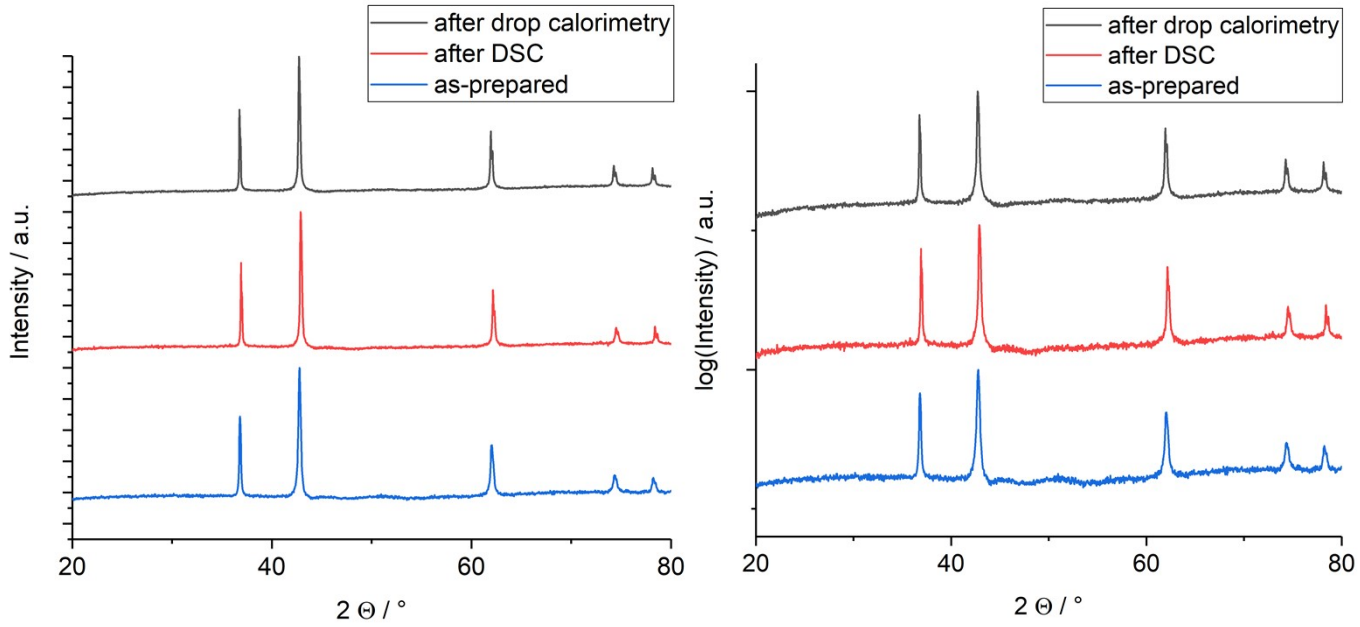

Fig. S1. XRD patterns, plotted in the Intensity (left) and log(Intensity) (right) coordinates, for the $(MgCoNiCuZn)_{0.2}O$ samples with different history: as-prepared (bottom lines), after DSC (middle lines) and after drop calorimetry (top lines)

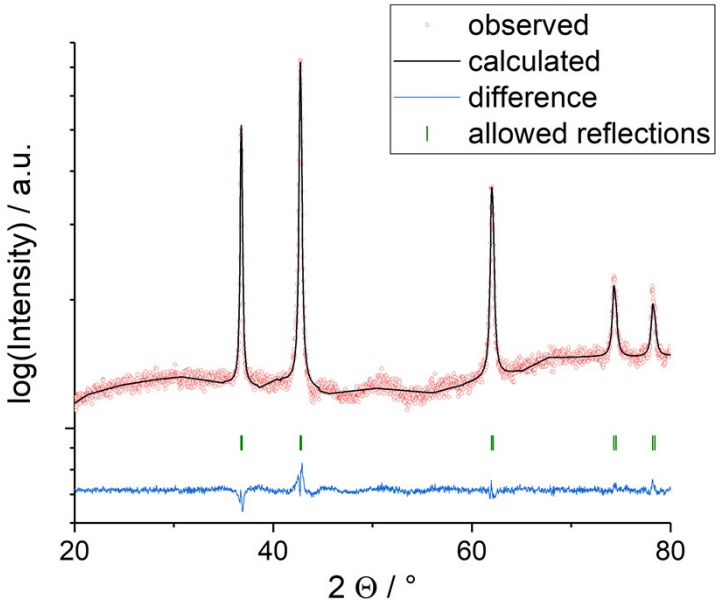

Fig. S2. Rietveld-refined XRD pattern for $(MgCoNiCuZn)_{0.2}O$ in the logarithmic coordinates: line is the calculated profile, circles – experimental pattern, bottom line – difference, vertical dashes – allowed Bragg reflections. The measurements were performed at (298.15 ± 5) K and (100 ± 3) kPa total pressure (expanded uncertainties, ≈95% confidence level). See also Fig. 1 in the main text.

2 Unsuccessful syntheses (SEM-EDS and XRD)

In this section, purely to point out the peculiarities of the process, which, we believe, are underrepresented in the literature, we give a few examples of the phase analysis of the samples with the target nominal composition "$(MgCoNiCuZn)_{0.2}O$".

The copper-deficient sample, whose XRD and elemental maps are shown in Figs. S3 (top) and S4 (top), respectively, was obtained by uniaxial pressing of the stoichiometric (with respect to "$(MgCoNiCuZn)_{0.2}O$") mixture of precursor oxides (MgO, Co_3O_4, NiO, CuO and ZnO), and then calcining the obtained bar on an alumina disc at 1573 K for 12 h with 100 K min^{-1} heating and cooling speeds. By the intense coloration of the disc support, it was evident that it reacted with the sample. Surprisingly, despite the fact that the sample was not quenched, no formation of the secondary tenorite or spinel phase typical of partially decomposed $(MgCoNiCuZn)_{0.2}O$ is seen in the XRD pattern. The pattern resembles the one for the single-phase $(MgCoNiCuZn)_{0.2}O$: it too can be indexed in $Fm\bar{3}m$ with a = 4.227 Å, and its FWHM is almost the same. Only the I_{111}/I_{200} ratio is significantly smaller in case of the sample 11745: 0.39, as compared with the 'perfect' value of 0.67. The elemental maps in Fig. S4 demonstrate uniform distribution of cations in the sample. However, the copper content in the sample is almost half of the expected value: the chemical formula would be $Mg_{0.25 \pm 0.03}Co_{0.22 \pm 0.01}Ni_{0.22 \pm 0.01}Cu_{0.10 \pm 0.01}Zn_{0.21 \pm 0.01}O$ if normalized by the sum of the cation concentrations.

These results also indicate that copper-deficient "$(MgCoNiCu_{1-x}Zn)_{0.2}O_{1-x}$" samples should be much more stable than the high-entropy $(MgCoNiCuZn)_{0.2}O$ oxide, which agrees with the literature [1–3]. We should also note that this experiment was performed before the publication of the study of Webb et al. [4] where the loss of copper from $(MgCoNiCuZn)_{0.2}O$ above 1573 K was reported. In their work, the samples were annealed on a sacrificial bed made of the same $(MgCoNiCuZn)_{0.2}O$ powder, which allowed them to observe the segregation of the copper-rich phases along the grain boundaries. In our case, the segregated copper reacted with the alumina support, so that the cation distribution in the rock-salt matrix phase remained uniform.

The XRD pattern and EDS data shown in Figs. S3 (middle) and S4 (bottom) were obtained for the sample synthesized in one step by annealing the uniaxially pressed pellets made of stoichiometric mixture of oxides (MgO, Co_3O_4, NiO, CuO and ZnO) at 1473 K for just 0.5 h before quenching. As seen, the secondary phases are hardly evident in the XRD pattern, which can be indexed in the $Fm\bar{3}m$ space group with a = 4.226 Å. However, the EDS results clearly show that the sample is not yet single-phase. The XRD pattern, as compared with the one for the single-phase $(MgCoNiCuZn)_{0.2}O$, is characterized by higher I_{111}/I_{200} ratio of 0.94 (which, however, is still less than unity) and somewhat higher FWHM. The average chemical composition, according to SEM, is close to the intended one: $Mg_{0.22 \pm 0.03}Co_{0.20 \pm 0.01}Ni_{0.20 \pm 0.01}Cu_{0.19 \pm 0.01}Zn_{0.19 \pm 0.01}O$.

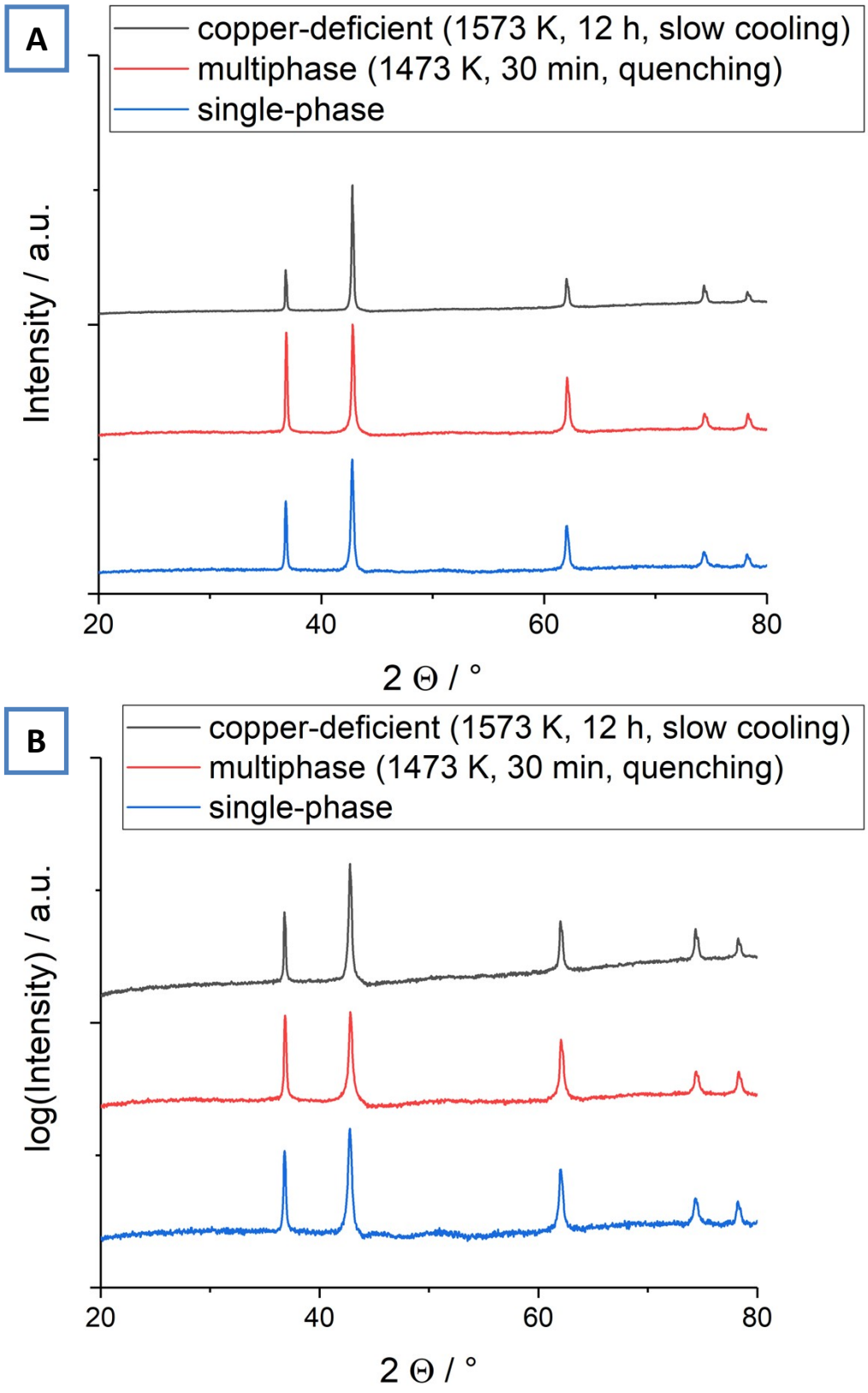

Fig. S3. XRD patterns, plotted in the Intensity (A) and log(Intensity) (B) coordinates, for the copper-deficient "$(MgCoNiCu_{1-x}Zn)_{0.2}O_{1-x}$" sample after annealing for 12 h at 1573 K and slow (100 K min^{-1}) cooling (top line), the "$(MgCoNiCuZn)_{0.2}O$" sample after annealing for 0.5 h at 1473 K and quenching (middle line), and the single-phase $(MgCoNiCuZn)_{0.2}O$ synthesized as described in the main text (bottom line)

Copper-deficient (1573 K, 12 h, slow cooling)

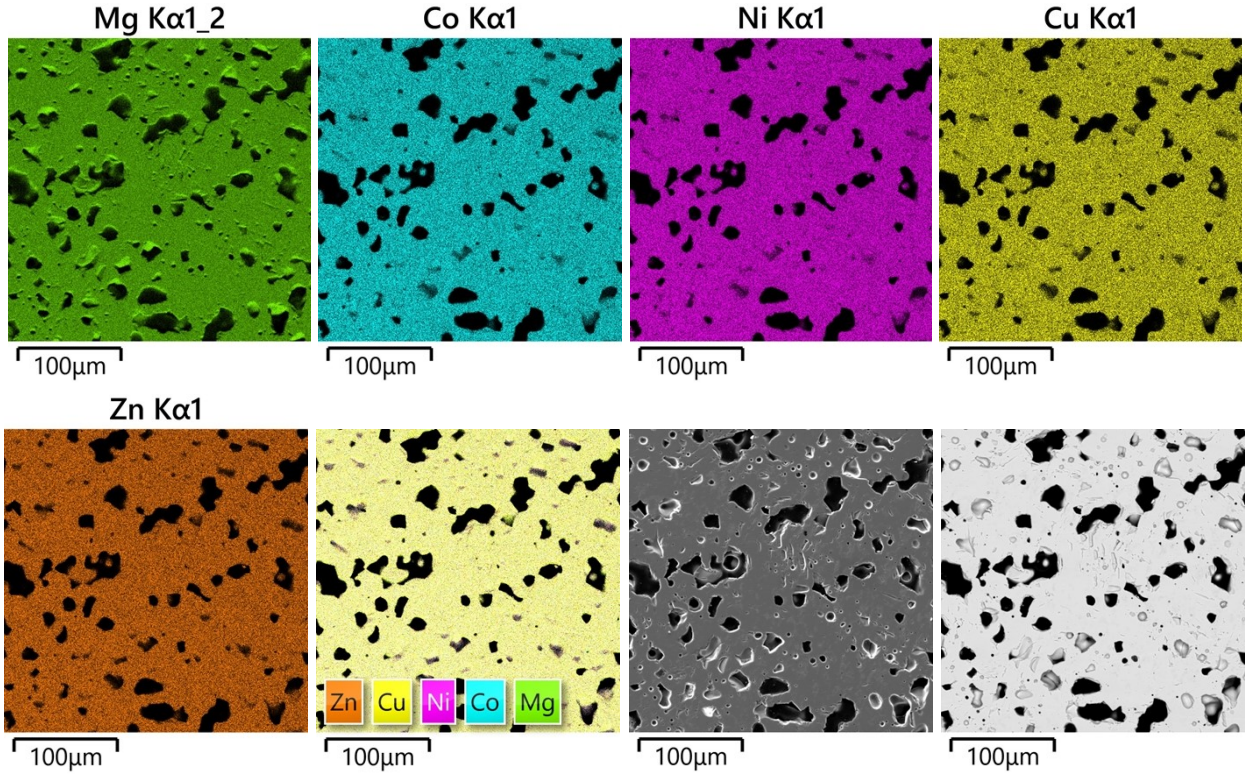

Multiphase (1473 K, 30 min, quenching)

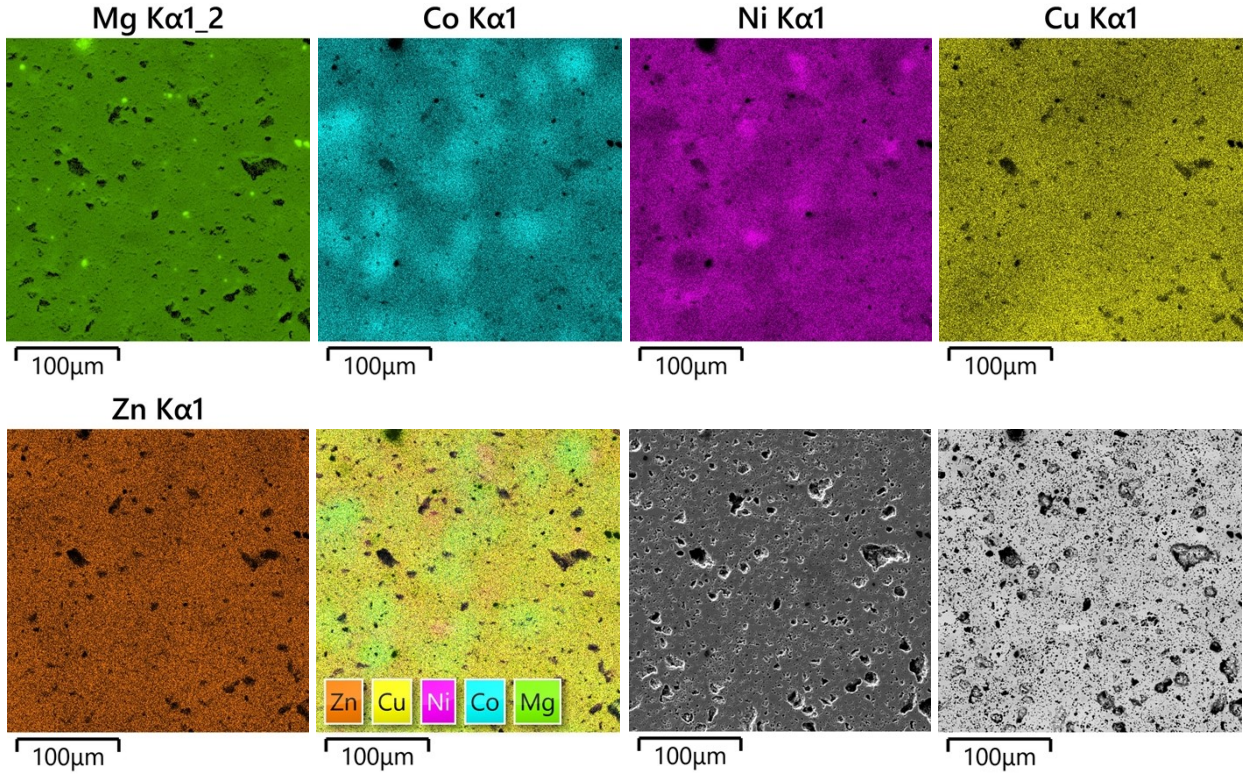

Fig. S4. EDS maps for the individual cations, layered EDS map, and SE and BSE images for the copper-deficient "$(MgCoNiCu_{1-x}Zn)_{0.2}O_{1-x}$" sample after annealing for 12 h at 1573 K and slow (100 K min^{-1}) cooling (top) and the "$(MgCoNiCuZn)_{0.2}O$" sample after annealing for 0.5 h at 1473 K and quenching (bottom)

3 Heat capacity (DSC, adiabatic calorimetry, drop calorimetry, and the literature data)

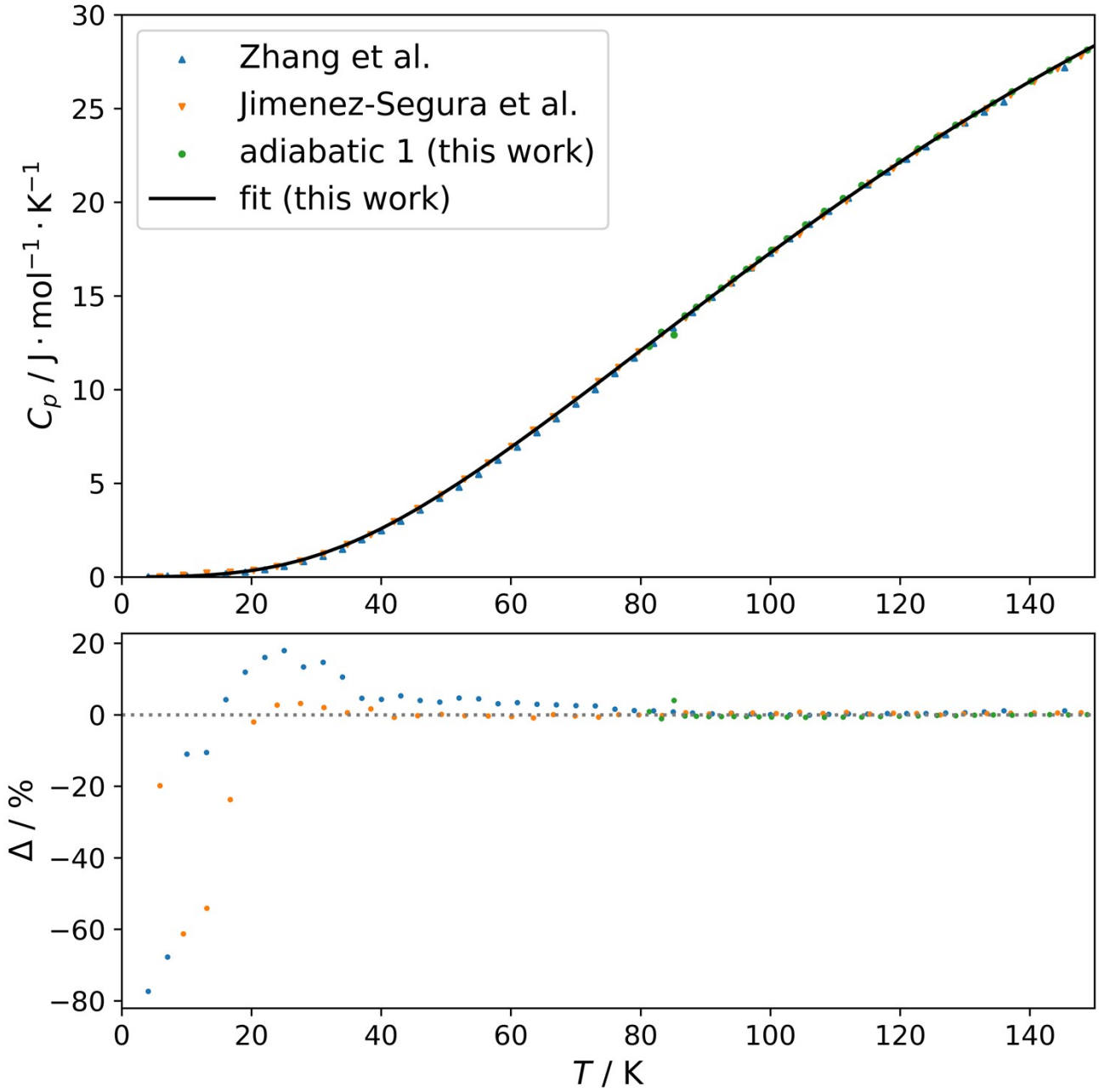

Fig. S5. Isobaric heat capacity, C_p, for $(MgCoNiCuZn)_{0.2}O$ at T up to 150 K and the difference between the smoothed function and the data $\Delta = 100(C_p(\text{fit}) - C_p(\text{exp})) / C_p(\text{exp})$ (bottom). Points: two series of adiabatic and DSC measurements (original data) and the relaxation calorimetry results ([5,6]). p = (100 ± 3) kPa total pressure (expanded uncertainty, ≈95% confidence level)

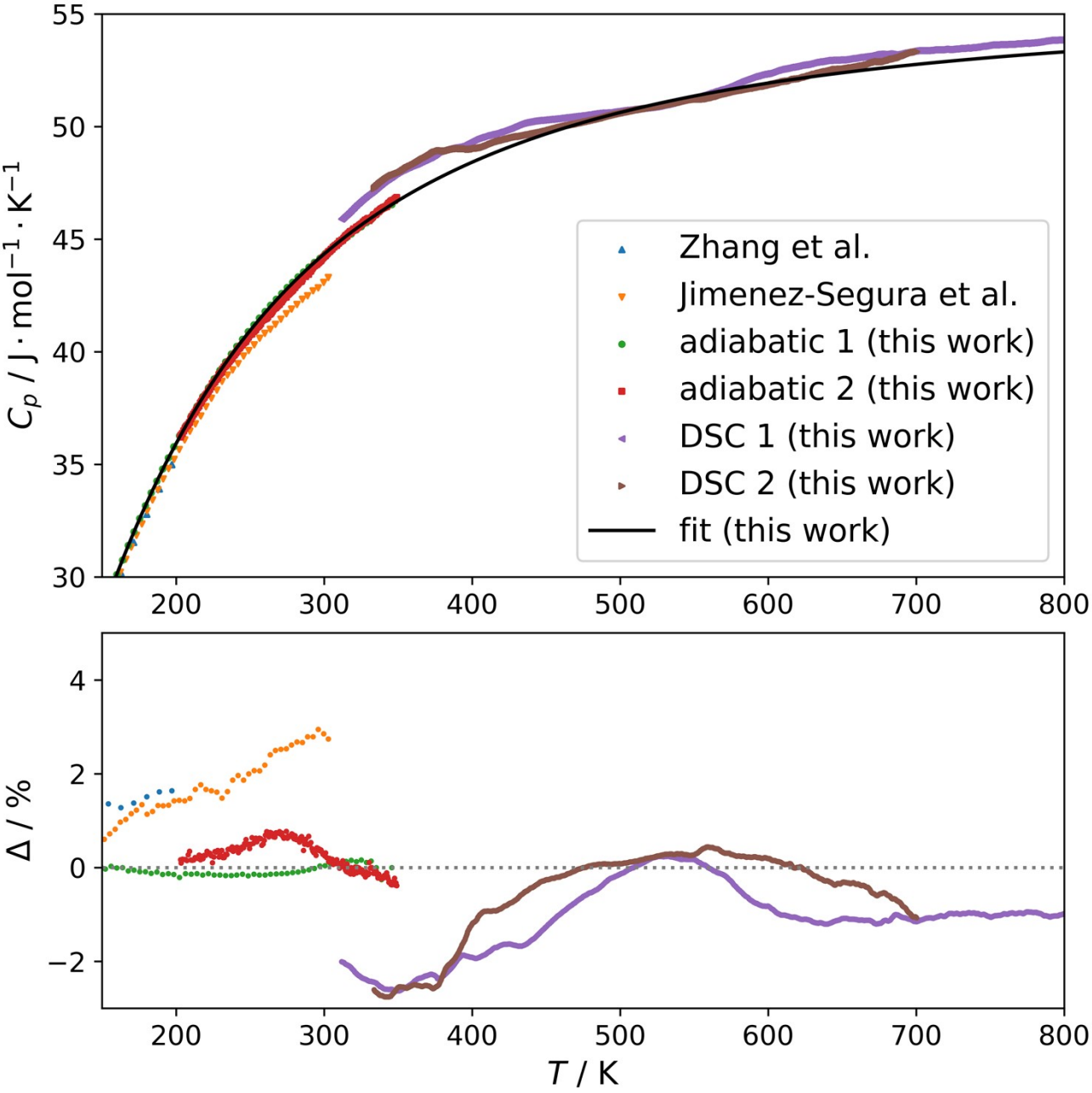

Fig. S6. Isobaric heat capacity, C_p, for $(MgCoNiCuZn)_{0.2}O$ at T between 150 K and 800 K and the difference between the smoothed function and the data $\Delta = 100(C_p(\text{fit}) - C_p(\text{exp})) / C_p(\text{exp})$ (bottom). Points: two series of adiabatic and DSC measurements (original data) and the relaxation calorimetry results ([5,6]). Solid black line: fitted function (see Eq. 3 in the main text). $p = (100 \pm 3)$ kPa total pressure (expanded uncertainty, ≈95% confidence level)

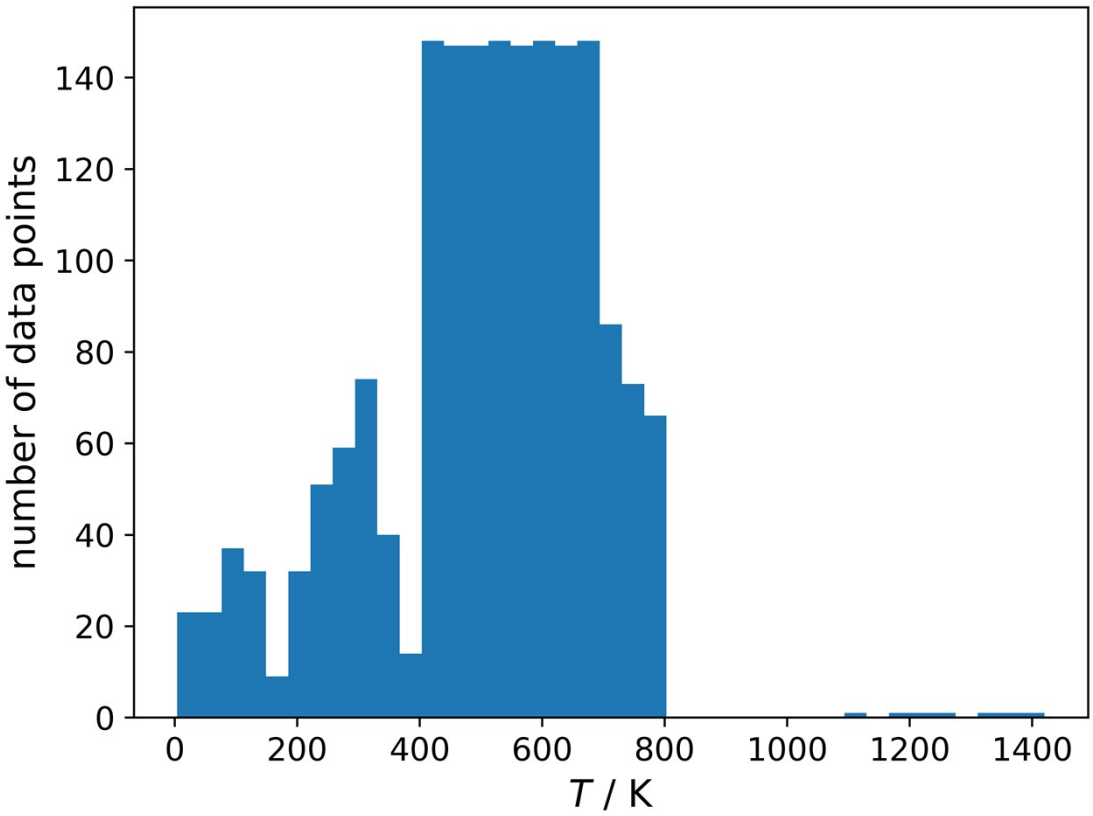

Fig. S7. Histogram of the heat capacity and enthalpy increment experimental data point distribution, including the original and the literature data [5,6] on both C_p and $\Delta_{Tlow}^{Thigh}H^\circ$

The following equation, which is of the same kind as the ones used in Robie and Hemingway [7],

$$C_p(T) = A_1 + A_2T + A_3T^{-2} + A_4T^{-0.5} + A_5T^2 \quad \text{(S1)}$$

reproduces the fitted C_p curve (one Debye and two Einstein terms, see Eq. 3 and Table 2 in the main text) within the temperature range of (293–1420) K with the maximum deviation of 0.02 J mol^{-1} K^{-1}. The coefficients in Eq. S1 are given in Table S3.

Table S3. Coefficients in Eq. S1 for the isobaric heat capacity function of single-phase rock-salt $(MgCoNiCuZn)_{0.2}O$

	A_1	A_2	A_3	A_4	A_5 [a]
Value	72.428	-0.008376	-394045.0	-370.488	2.043E-6
Uncertainty [b]	0.116	0.000075	2314.8	2.082	0.023E-6

[a] the exponential form 2.043E-6 = $2.043 \cdot 10^{-6}$ is given to facilitate the copying

[b] The uncertainties are the values of the standard error (1 σ) found during the fitting. The "extra" significant digits for both the values and the uncertainties are given to decrease the rounding errors in the calculations.

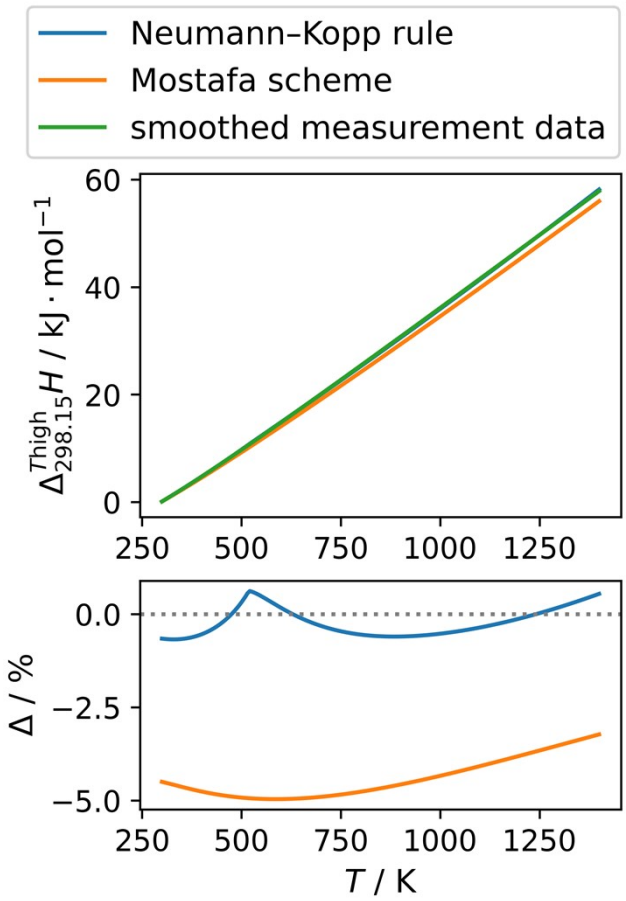

Fig. S8. Enthalpy increments, $\Delta_{298.15\,K}^{Thigh}H^{\circ}$, of $(MgCoNiCuZn)_{0.2}O$ calculated from the smoothed experimental $C_p(T)$ (see Eq. 3 and Table 2) in comparison with their predictions calculated with the Neumann–Kopp rule and the group contribution scheme of Mostafa et al. [8]

4 Thermogravimetric analysis of $(MgCoNiCuZn)_{0.2}O$

The results of three additional TG experiments are given in Fig. S9 below. The 1st, 2nd and 3rd panes (from top to bottom) in Fig. S9 correspond to the experiments that are designated as "first", "second" and "third" in the text below. These experiments show the reproducibility of the oxygen content in the calorimetric measurements, confirming that the measurements up to 1423 K correspond to the $(MgCoNiCuZn)_{0.2}O$ sample with negligible oxygen nonstoichiometry.

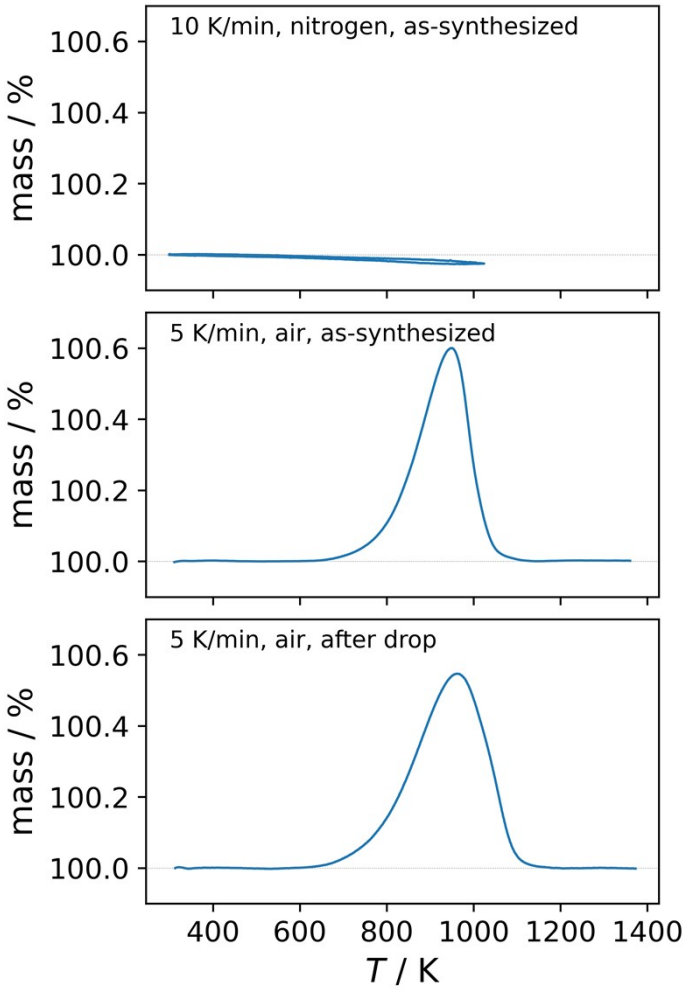

Fig. S9. Thermogravimetric analysis results for $(MgCoNiCuZn)_{0.2}O$:
heating and cooling of the as-synthesized sample in nitrogen (top pane), heating of the as-synthesized sample in air (center pane) and heating of the sample after all the drop experiments (bottom pane) at the total pressure of (100 ± 3) kPa (expanded uncertainty, ≈95% confidence level)

The first experiment follows the same measurement mode as the DSC heat capacity measurements: 10 K min^{-1} heating and cooling speed, 25 ml min^{-1} flow of dry nitrogen, Sensys 830 (Setaram, France) setup. As seen in the upper pane in Fig. S9 where both heating and cooling curves are plotted, no decomposition takes place. A very small, less than 0.03% at all temperatures, reversible mass loss can be attributed to the oxygen nonstoichiometry of the sample. The magnitude of the mass loss at temperatures below 800 K, where the DSC measurements of C_p were performed, corresponds to the oxygen nonstoichiometry index $\delta < 0.001$ in $(MgCoNiCuZn)_{0.2}O_{1-\delta}$, which can be regarded as negligible.

The second and the third TG measurements were performed with 5 K min^{-1} heating speed in dry air (50 ml min^{-1} flow) on an STA 409 PC (Netzsch, Germany) setup. In these experiments only the samples were different. In the 2nd measurement, the as-synthesized sample was taken, and in the 3rd – the sample that after all the drop experiments was annealed at 1423 K in air for up to 1 h and then quenched to room temperature, i.e., prepared in the same way as we prepared the samples before each drop calorimetry experiment.

The most prominent feature in the second and third plots in Fig. S9 is the broad peak in the temperature region where $(MgCoNiCuZn)_{0.2}O$ is unstable in air. The peak is due to the oxygen uptake, occurring when the sample decomposes with the spinel phase formation, and the subsequent oxygen loss, which happens when the secondary phases decompose and the corresponding cations are incorporated again into the rock-salt crystal lattice of $(MgCoNiCuZn)_{0.2}O$ [9,10].

For the present discussion, however, the mass values "before" and "after" the decomposition are of more importance. As seen in Fig. S9, the initial masses (at low *T*, where $(MgCoNiCuZn)_{0.2}O$ is metastable) and the masses at high temperatures (where $(MgCoNiCuZn)_{0.2}O$ is stable) are the same for both the as-synthesized sample and the sample after the drop calorimetry, which means that the oxygen nonstoichiometry in all these samples is also the same. If, for example, the sample reannealed after the drop experiments (bottom pane in Fig. S9) had possessed different nonstoichiometry, its mass would not have returned to the same level as the initial mass before heating. This confirms the reproducibility of the oxygen content in $(MgCoNiCuZn)_{0.2}O$ in our drop calorimetric experiments.

We would like to mention that we are not the first to perform these kinds of TG measurements for $(MgCoNiCuZn)_{0.2}O$, and that our conclusions are in agreement with those of Jacobson et al. [10].

5 Contributions to the entropy of mixing in $(MgCoNiCuZn)_{0.2}O$

The following reaction is the same as reaction (6) in the main text:

$$0.2MgO\ (T,\ RS) + 0.2CoO\ (T,\ RS) + 0.2NiO\ (T,\ RS) + 0.2CuO\ (T,\ T) + 0.2ZnO\ (T,\ W) = (MgCoNiCuZn)_{0.2}O\ (T,\ RS) \quad \text{(S2)}$$

where T is the temperature, the high-entropy product is in its rock-salt (RS) solid phase, and all the other oxides – in the most stable solid states: rock-salt (RS), tenorite (T) or wurtzite (W).

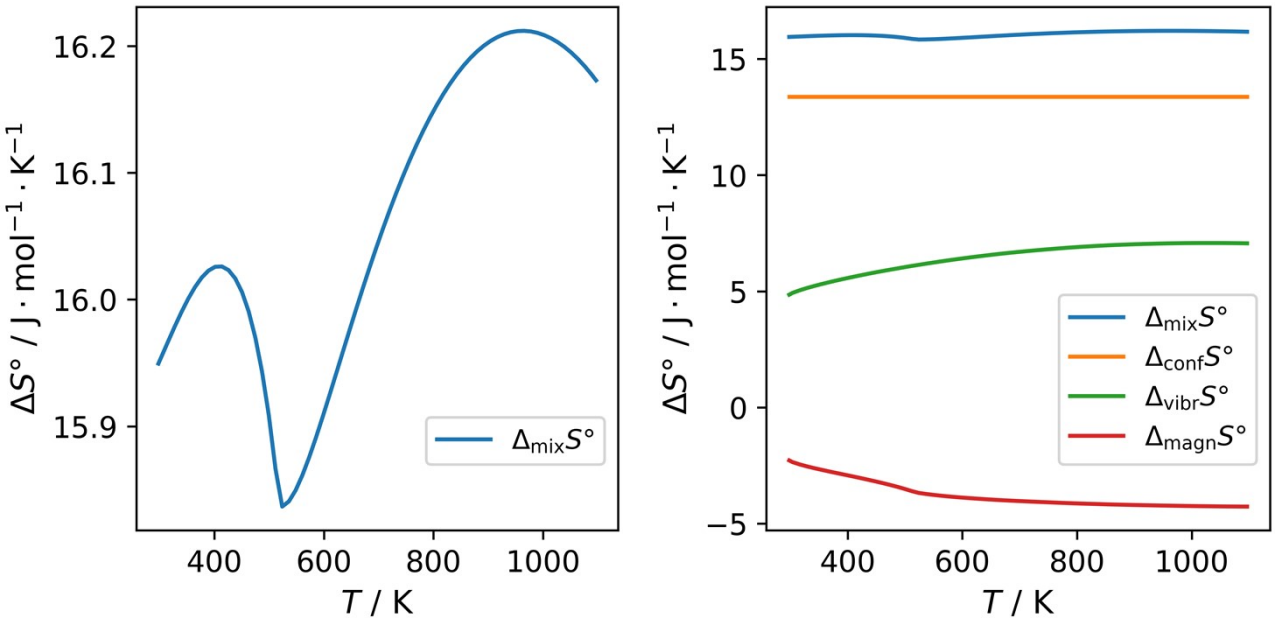

Fig. S10. Vibrational, $^{\Delta_{vibr}}S_T^{\circ}$, configurational, $^{\Delta_{conf}}S_T^{\circ}$, and magnetic, $^{\Delta_{magn}}S_T^{\circ}$, contributions to the total entropy of mixing, $^{\Delta_{mix}}S_T^{\circ}$ (the entropy change in reaction (S2)), calculated based on the results of this work and refs.[11–15] (see Eqns. (8)-(9) in Section 3.5 of the main text)

References

[1] S.S.I. Almishal, J.T. Sivak, G.N. Kotsonis, Y. Tan, M. Furst, D. Srikanth, V.H. Crespi, V. Gopalan, J.T. Heron, L.-Q. Chen, C.M. Rost, S.B. Sinnott, J.-P. Maria, Untangling individual cation roles in rock salt high-entropy oxides, Acta Mater. 279 (2024) 120289. https://doi.org/10.1016/j.actamat.2024.120289.

[2] G. Anand, A.P. Wynn, C.M. Handley, C.L. Freeman, Phase stability and distortion in high-entropy oxides, Acta Mater. 146 (2018) 119–125. https://doi.org/10.1016/j.actamat.2017.12.037.

[3] M. Fracchia, M. Coduri, S. Bonati, C. Dejoie, P. Ghigna, U. Anselmi-Tamburini, Beyond configurational entropy: the role of solubility equilibria in the stability of the system (Co,Cu,Mg,Ni,Zn)O, J. Eur. Ceram. Soc. 45 (2025) 117237. https://doi.org/10.1016/j.jeurceramsoc.2025.117237.

[4] M. Webb, M. Gerhart, S. Baksa, S. Gelin, A.-R. Ansbro, P.B. Meisenheimer, T. Chiang, J.-P. Maria, I. Dabo, C.M. Rost, J.T. Heron, High temperature stability of entropy-stabilized oxide $(MgCoNiCuZn)_{0.2}O$ in air, Appl. Phys. Lett. 124 (2024). https://doi.org/10.1063/5.0199076.

[5] M.P. Jimenez-Segura, T. Takayama, D. Bérardan, A. Hoser, M. Reehuis, H. Takagi, N. Dragoe, Long-range magnetic ordering in rocksalt-type high-entropy oxides, Appl. Phys. Lett. 114 (2019) 122401. https://doi.org/10.1063/1.5091787.

[6] J. Zhang, J. Yan, S. Calder, Q. Zheng, M.A. McGuire, D.L. Abernathy, Y. Ren, S.H. Lapidus, K. Page, H. Zheng, J.W. Freeland, J.D. Budai, R.P. Hermann, Long-Range Antiferromagnetic Order in a Rocksalt High Entropy Oxide, Chem. Mater. 31 (2019) 3705–3711. https://doi.org/10.1021/acs.chemmater.9b00624.

[7] R. Robie, B. Hemingway, Thermodynamic properties of minerals and related substances at 298.15 K and 1 bar (10^5 pascals) pressure and at higher temperatures, 1995. https://doi.org/10.3133/b2131.

[8] A.T.M.G. Mostafa, J.M. Eakman, M.M. Montoya, S.L. Yarbro, Prediction of Heat Capacities of Solid Inorganic Salts from Group Contributions, Ind. Eng. Chem. Res. 35 (1996) 343–348. https://doi.org/10.1021/ie9501485.

[9] C.M. Rost, E. Sachet, T. Borman, A. Moballegh, E.C. Dickey, D. Hou, J.L. Jones, S. Curtarolo, J.-P. Maria, Entropy-stabilized oxides, Nat. Commun. 6 (2015) 8485. https://doi.org/10.1038/ncomms9485.

[10] V. Jacobson, K. Gann, M. Sanders, G. Brennecka, Densification of the entropy stabilized oxide $(Mg_{0.2}Co_{0.2}Ni_{0.2}Cu_{0.2}Zn_{0.2})O$, J. Eur. Ceram. Soc. 42 (2022) 4328–4334. https://doi.org/10.1016/j.jeurceramsoc.2022.04.017.

[11] C.W. Bale, E. Bélisle, P. Chartrand, S.A. Decterov, G. Eriksson, A.E. Gheribi, K. Hack, I.H. Jung, Y.B. Kang, J. Melançon, A.D. Pelton, S. Petersen, C. Robelin, J. Sangster, P. Spencer, M.A. Van Ende, FactSage thermochemical software and databases, 2010–2016, Calphad 54 (2016) 35–53. https://doi.org/10.1016/j.calphad.2016.05.002.

[12] J.R. Taylor, A.T. Dinsdale, A Thermodynamic Assessment of the Ni-O, Cr-O and Cr-Ni-O Systems Using the Ionic Liquid and Compound Energy Models / Eine thermodynamische Optimierung der Systeme Ni-O, Cr-O und Cr-Ni-O durch das Modell der Ionenschmelze und das Untergittermodell, Int. J. Mater. Res. 81 (1990) 354–366. https://doi.org/10.1515/ijmr-1990-810509.

[13] M. Chen, B. Hallstedt, L.J. Gauckler, Thermodynamic assessment of the Co-O system, J. Phase Equilibria 24 (2003) 212–227. https://doi.org/10.1361/105497103770330514.

[14] E. Gmelin, U. Köbler, W. Brill, T. Chattopadhyay, S. Sastry, Magnetic specific heat and susceptibility of cupric oxide (CuO) single crystals, Bull. Mater. Sci. 14 (1991) 117–123. https://doi.org/10.1007/BF02747301.

[15] B.A. Frandsen, K.A. Petersen, N.A. Ducharme, A.G. Shaw, E.J. Gibson, B. Winn, J. Yan, J. Zhang, M.E. Manley, R.P. Hermann, Spin dynamics and a nearly continuous magnetic phase transition in an entropy-stabilized oxide antiferromagnet, Phys. Rev. Mater. 4 (2020) 074405. https://doi.org/10.1103/PhysRevMaterials.4.074405.